analytical chemistry

pubs.acs.org/ac

Technical Note

3D Printed Instrument for Taylor Dispersion Analysis with Two-Point Laser-Induced Fluorescence Detection

Meagan R. Moser, Claire M. Smith, Genoveve G. Gutierrez, and Christopher A. Baker*

Cite This: *Anal. Chem.* 2022, 94, 6089−6096

Read Online

ACCESS | Metrics & More | Article Recommendations | Supporting Information

ABSTRACT: Precisely controlling the size of engineered biomolecules and pharmaceutical compounds is often critical to their function. Standard methods for size characterization, such as dynamic light scattering or size exclusion chromatography, can be sample intensive and may not provide the sensitivity needed for mass- or concentration-limited biological systems. Taylor dispersion analysis (TDA) is a proven analytical method for direct, calibration-free size determination which utilizes only nL-pL sample volumes. In TDA, diffusion coefficients, which are mathematically transformed to hydrodynamic radii, are determined by characterizing band broadening of an analyte under well-controlled laminar flow conditions. Here, we describe the design and development of a 3D printed instrument for TDA, which is the first such instrument to offer dual-point laser-induced fluorescence (LIF) detection. The instrument utilized a fully 3D printed eductor as a vacuum source for precise and stable pressure-driven flow within a capillary, evidenced by a linear response in generated static pressure to applied gas pressure (R^2 = 0.997) and a 30-fold improvement in stability of static pressure (0.05% RSD) as compared to a standard mechanical pump (1.53%). Design aspects of the LIF detection system were optimized to maximize S/N for excitation and emission optical axes, and high sensitivity was achieved as evidenced by an 80 pM limit of detection for the protein R-Phycoerythrin and low nM limits of detection for three additional fluorophores. The utility of the instrument was demonstrated via sizing of R-Phycoerythrin at pM concentrations.

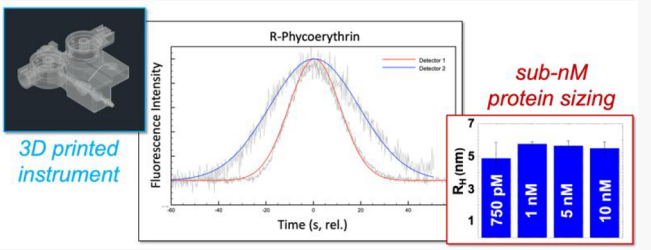

INTRODUCTION

Macromolecular products for biological and pharmaceutical applications, such as liposomes, nanoparticles, engineered proteins, and drug delivery systems, may require precise control over product size to achieve desired material properties. The design and development of new macromolecular materials can benefit from the availability of simple, rapid, sensitive, and high accuracy analytical methods for size characterization. Many common size characterization techniques require extensive method development, tedious sample preparation, large sample volumes, or lengthy analysis times.[1] Two widely used methods for size characterization are dynamic light scattering (DLS) and size exclusion chromatography (SEC). DLS provides rapid measurements with limited sample preparation but is biased in sensitivity toward large particles and aggregates.[2] For example, Hawe et al. used DLS to measure a range of concentrations (0.05−50 mg mL^{-1}) of several proteins and peptides.[3] Though DLS successfully sized the antibody drug adalimumab (5−6 nm) at the lowest concentration, it was not possible to size the peptide oxytocin (∼0.8 nm) at similar concentrations. SEC requires calibration and is susceptible to analyte-column interactions dependent on mobile phase composition.[4] Ricker and Sandoval examined various operational parameters, such as column length, flow rate, sample volume, and mobile phase conditions, and their effects on SEC separation performance.[5] They demonstrated the susceptibility of SEC methods to deleterious effects related to mobile phase ionic strength and pH while analyzing mouse myeloma antibodies with differing charges. Such electrostatic and hydrophobic effects can ultimately result in inaccuracies of hydrodynamic radius (R_H) measured by SEC. Though various solvent additives and organic modifiers have been utilized to suppress adsorption and hydrophobic interactions in SEC,[4,6−9] extensive method development is still often required to obtain accurate sizing.

Taylor dispersion analysis (TDA) offers similar sizing capabilities to DLS and SEC, while utilizing nL sample volumes and without the need for size-based calibration or comparison to size standards. First described in 1953,[10] TDA enables direct determination of molecular diffusion coefficients (D's) across a wide dynamic range of R_H from Å to μm. Taylor dispersion arises from the interplay of radial diffusion within a cylindrical flow channel and the parabolic velocity profile of pressure-driven laminar flow in such flow systems. As a result, a sample zone will spread out axially, the degree of which can be observed by

Received: October 21, 2021
Accepted: March 24, 2022
Published: April 13, 2022

characterizing band broadening of a sample zone under continuous flow. D is inversely proportional to an analyte's R_H, and therefore, the rate of band broadening by Taylor dispersion is influenced directly by the analyte's R_H. TDA is a mathematical framework for extracting diffusion coefficients directly from the observed rates of band broadening due to Taylor dispersion.

TDA has evolved from studying gaseous diffusion coefficients in large tubes[11] to capillary-based solution phase measurements of small molecules,[12,13] macromolecular complexes,[14−16] and even micron-scale particles.[17] In TDA, analysis time is proportional to the square of the tubing radius. Thus, small molecule analytes flowing through a tube of 1 mm radius would require several hours to produce the same degree of Taylor dispersion observed in a 50 μm radius capillary in only minutes.[18] Reduced analysis times, improved precision of flow rate control, and low sample consumption have all motivated the use of capillary electrophoresis (CE) instrumentation for performing TDA. To highlight these benefits, our group recently reviewed the theory and applications of TDA performed in fused silica capillaries.[1]

Highlighting the need for continuous flow velocity in TDA, Sharma et al. described the effects of the initial ramp in flow velocity that occurs upon pressure application in CE instruments, finding the pressure ramp to be a source of error in TDA analyses with short elution times.[18] Discontinuous flow velocities, therefore, presented the need for empirical mathematical corrections. Measurement errors as high as 40% have been attributed to such suboptimal flow conditions.[19] To address these limitations, dual-point detector schemes have been developed that allow TDA to be conducted under continuous flow.[12,20−22]

Chamieh et al. addressed the engineering challenge of integrating dual-point detection into commercial CE instrumentation by modifying the optical detection interface within an Agilent CE cassette such that the capillary could be looped within the cassette and pass the UV detection point twice;[21] however, this detection scheme resulted in substantially reduced sensitivity compared to the conventional UV detection system. Our group developed an LED-induced fluorescence detection system for integration into commercial CE instrumentation, enabling dual point detection with higher sensitivity than is possible by UV absorbance detection,[22] achieving a detection limit of 613 ± 13 pM for fluorescein. While LED-induced fluorescence offered improved sensitivity over UV absorbance detection, these detection limits were still modest in comparison to those achievable by laser-induced fluorescence (LIF) detection. LIF combines low concentration limits of detection (typ. mid-to-low pM) with highly selective detection often achieved by selective fluorescent labeling, making it a powerful detection mode for nL and smaller sample volumes, such as in capillary and microfluidic applications.[23−27] The combination of detection sensitivity and selectivity makes LIF detection well suited for targeted analyses, such as in immunoassays[28,29] and by selective fluorescent probe chemistries.[30,31]

To deliver improved instrumentation for capillary TDA and to enable wider adoption of TDA as a sizing technique, here we describe the design and optimization of a 3D printed instrument for TDA with dual-point LIF detection. The instrument utilized a fully 3D printed eductor as a vacuum source for precise and stable pressure-driven flow within the capillary. A LIF detection system was developed based on a 3D printed architecture for holding optical elements in alignment with the capillary. Design aspects of the LIF detection system were optimized to maximize S/N, and the utility of the high sensitivity TDA instrument was demonstrated via protein sizing at pM concentrations.

MATERIALS AND METHODS

Reagents and Materials. Rhodamine 6G 99% was the ACROS Organics brand from Fisher Scientific (Suwannee, GA). R-Phycoerythrin was purchased from AnaSpec, Inc. (Fremont, CA), AlexaFluor 532 was purchased from Thermo-Fisher Scientific (Waltham, MA), and CF532 was purchased from Biotium (Hayward, CA). Phosphate buffered saline (PBS) was the Fisher BioReagents brand and was purchased from Fisher Scientific (Suwannee, GA). All aqueous solutions were prepared using DI water. Fused silica capillary was the Polymicro brand purchased from Fisher Scientific (Suwannee, GA). 3D printing materials and procedures are described in the Supporting Information.

Eductor Pressure System Characterization. To characterize the vacuum pressure system, the eductor component was 3D printed separately. The gas inlet was connected to house nitrogen, and the vacuum inlet was connected to a 5 ft length of 1/8″ i.d., 1/4″ o.d. vinyl tubing. The nitrogen line was set to varying gauge pressures (2−10 psig), and mmH_2O was recorded by measuring the height of a water column drawn by the eductor vacuum pressure. mmH_2O was mathematically converted to psi for calibration plots, and inlet nitrogen pressures were converted to volumetric flow rates, as described in the Supporting Information. Pressure stability was characterized by recording a video of the water column and using ImageJ in combination with a custom MatLab script to track the water column height over time.

LIF Detection System. Laser excitation was provided by two 532 nm collimated laser diode modules (CPS532, Thorlabs, Newton, NJ) and focused on the capillary detection windows via integrated 3D printed pinholes and 9.0 mm diameter 20 mm FL plano convex lenses (LA1472, Thorlabs Inc., Newton, NJ). Fluorescence emission was collected via a 6.0 mm N-BK7 ball lens (Edmund Optics Inc., Barrington, NJ) and a 10 mm FL 25 mm diameter concave mirror (43464, Edmund Optics Inc., Barrington, NJ) for transmission to a Hamamatsu H7828-50 photomultiplier module fitted with an OD 0.9 neutral density filter (NE09B, Thorlabs Inc., Newton, NJ), 533/17 nm OD 6 notch filter (NF533-17, Thorlabs Inc., Newton, NJ), 580 ± 2, fwhm 10 ± 2 nm OD 6 bandpass filter (FB580-10, Thorlabs Inc., Newton, NJ), 550 nm OD 6 long-pass filter (FELH0550, Thorlabs Inc., Newton, NJ), 50 mm focusing lens (LA1131, Thorlabs Inc., Newton, NJ), and 532 nm OD 5 notch filter. Data acquisition was via a USB DAQ module (USB-6341, National Instruments, Austin, TX) with software written in-house in LabView (National Instruments, Austin, TX).

Validation of TDA Using Model Fluorescent Molecules. Taylor dispersion experiments were carried out in a 25.5 cm length, 100 μm i.d./360 μm o.d. fused-silica capillary with 15 cm detection window spacing. Samples of AlexaFluor 532 and R-Phycoerythrin (R-PE) were prepared with 1X PBS buffer. A flow rate calibration was performed with the selected capillary size and window spacing (Supporting Information, Figure S-1) to determine the input eductor pressure needed to satisfy the Taylor conditions. Specific flow procedures for TDA experiments are described in the Supporting Information. Flow conditions for TDA experiments were selected to limit flow-related measurement errors to 3% or lower.[32] Resulting peaks were fitted to Gaussian functions, and differences in arrival time

https://doi.org/10.1021/acs.analchem.1c04566
Anal. Chem. 2022, 94, 6089−6096

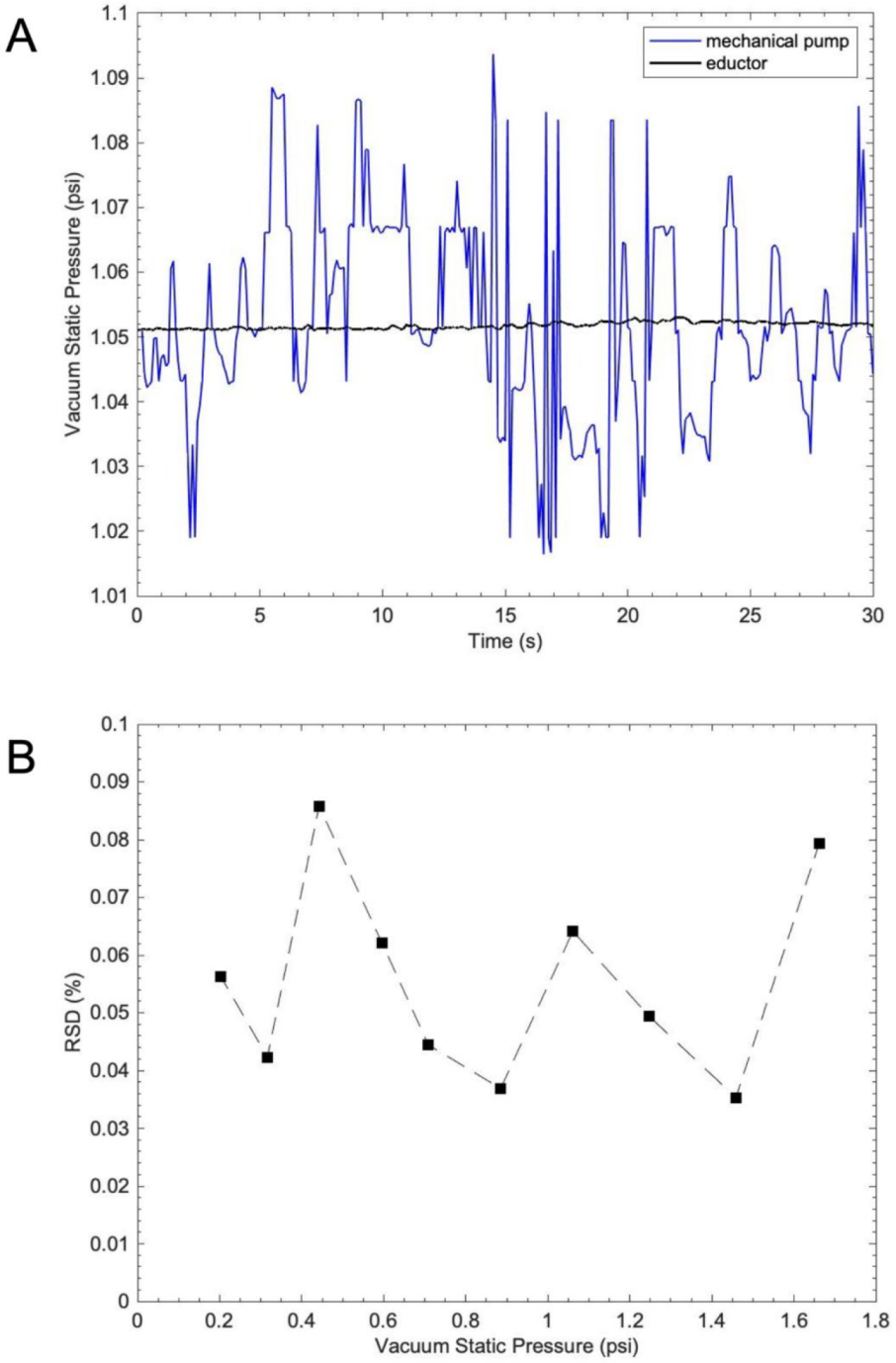

Figure 1. Eductor pressure stability. (A) Comparison of vacuum pressure stability over time for an eductor (black trace, 0.05%) and diaphragm pump (blue trace, 1.53% RSD). (B) Static pressure stability expressed as percent relative standard deviation over a range of applied inlet gas pressures. Average RSD = 0.055%.

and peak variance at the two detection points were used to calculate the diffusion coefficient and hydrodynamic radius. Values were tested for outliers using Grubb's test. At a confidence interval of 95%, two data points were eliminated as outlying values from data collected with 5 nM and 1 nM R-PE.

RESULTS

Commercial CE instrumentation provides convenient and precise control of flow rates in capillaries, but significant barriers to adopting capillary TDA exist including instrumental cost and the lack of available dual-point LIF detection. To reduce these barriers, we have developed a 3D printed instrument for TDA that combines accurate capillary positioning, precise flow control at low flow rates, and two-point LIF detection.

Capillary Positioning. Precise control of capillary length and the distance between detection points are key to accurate measurements by TDA because they influence the precision of observation time (t_R) and the volumetric flow rate (u), both of which are critical to satisfying the Taylor conditions.[1] The instrument design utilized the geometric precision of 3D printing to achieve accurate detection window positioning via capillary cartridges designed for three specific detection window

https://doi.org/10.1021/acs.analchem.1c04566
Anal. Chem. 2022, 94, 6089−6096

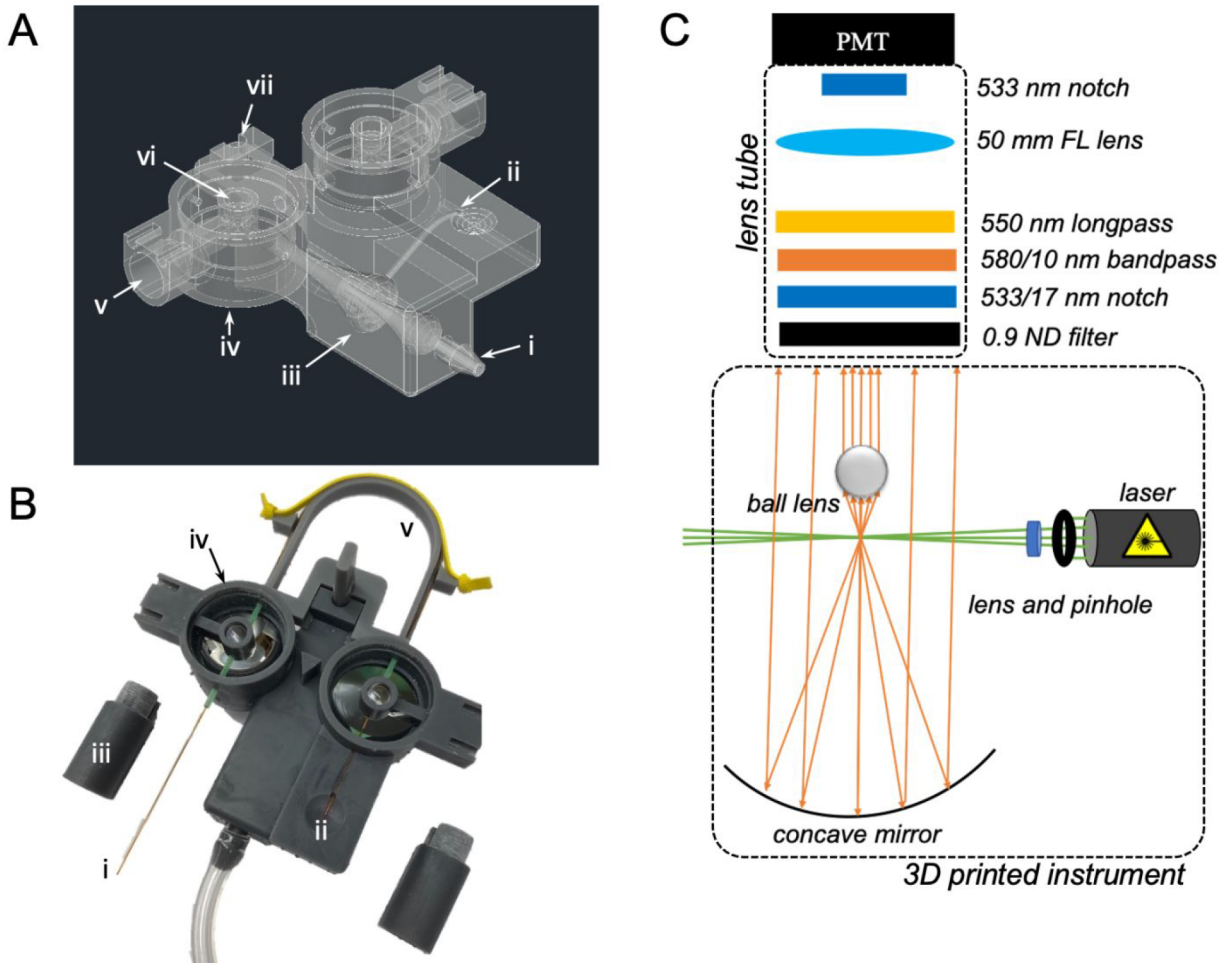

Figure 2. Design illustrations of the 3D printed TDA instrument. (A) 3D CAD rendering of the primary instrument body illustrating the eductor control compressed air inlet (i), eductor vacuum channel (ii), internal eductor geometry (iii), mounting location of the objective mirror (iv), mounting location of excitation optics (v), mounting location of the objective ball lens (vi), and mounting location of the 3D printed capillary cartridge (vii). (B) Photograph of the assembled instrument, illustrating the capillary inlet (i), capillary outlet with dish geometry to catch effluent (ii), detachable laser module mount (iii), mounting location of lens tube containing emission/detection optics (iv), and 3D printed capillary cartridge (v). (C) Schematic illustration of the optical design in the optimized excitation and emission axes.

spacings: 10, 15, and 25 cm (Supporting Information, Figure S-2). To prepare a capillary cartridge with appropriately spaced detection windows, an accompanying 3D printed alignment tool was produced (Supporting Information, Figure S-2) to indicate precise locations of detector windows and cutting locations (Supporting Information, Figure S-2, red arrows) at the capillary inlet and outlet. Capillary cartridges mounted to the alignment tool with the same dovetail joint utilized on the instrument body. Thus, once the capillary is prepared, the cartridge is removed from the alignment tool, placed onto the instrument body, and secured with a 3D printed key (Supporting Information, Figure S-2, red box) to ensure that the placement of the detection windows aligns appropriately with excitation and detection optics within the 3D printed LIF detector system.

While the cartridge and alignment tool ensured appropriate detection window positioning in the longitudinal dimension of the capillary, lateral positioning of the capillary within the focal volumes of excitation and collection optics was also critical. Typical consumer grade 3D printing resolution is not sufficient to produce features small enough to define lateral positioning of the 360 μm o.d. capillary within the detection volume. A simple approach to achieve appropriate lateral positioning was the use of capillary tubing sleeves of the type utilized to interface capillaries with 1/16″ fingertight fittings. Thus, the opening to accept the capillary into the 3D printed detectors was sized to fit the outer diameter of these tubing sleeves, and then sleeves were inserted to ensure that the capillary was centered on the intended axis through the middle of the detector (Supporting Information, Figure S-3).

The capillary cartridge is designed to enable ambient air flow in the vicinity of the mounted capillary. Temperature regulation is critical for TDA, since temperature fluctuations perturb solution viscosity. We observed no substantial source of thermal energy input, as no electric field was applied to the capillary, the laser excitation sources were IR filtered, and they were observed to operate at ambient temperature. Thus, with consideration for the efficient heat dissipating qualities of fused silica capillaries, we deemed this passive cooling approach to be sufficient. In future applications, further cooling measures may be warranted, especially if different excitation sources are used or experiments require the application of an electric field to the capillary.

Eductor-Driven Pressure System. Achieving accurate TDA with relatively short capillary lengths required precise and stable control of pressure-driven flow at low nL min^{-1}

https://doi.org/10.1021/acs.analchem.1c04566
Anal. Chem. 2022, 94, 6089−6096

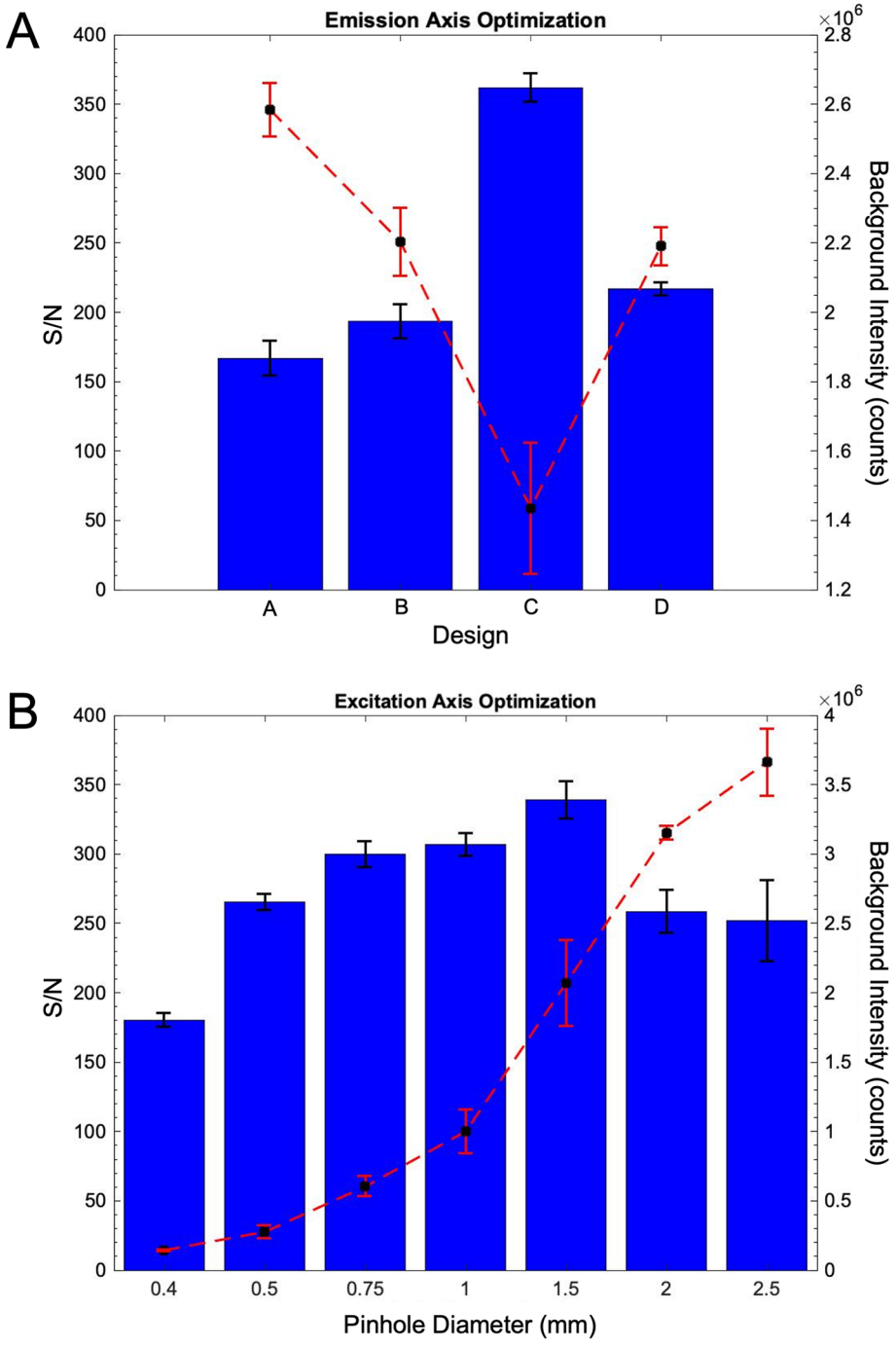

Figure 3. Excitation and emission axis optimizations. (A) Results of emission axis optimization, including comparison of S/N and background counts for designs A−D. (B) S/N and background counts as a function of the pinhole diameter in the excitation axis. A pinhole diameter of 1.5 mm produced the greatest S/N ratio. At a 2.5 mm pinhole diameter, 500 nM analyte concentration produced a detector response that exceeded the dynamic range of the PMT; therefore, the data shown is a 2-fold extrapolation of data collected for an analyte concentration of 250 nM.

volumetric flow rates. At the core of the instrument design is a fully 3D printed eductor, designed to generate subambient pressure at the capillary outlet and, therefore, drive pressure-driven flow through the capillary with an open and accessible capillary inlet. Eductors operate on the Bernoulli principle and have been employed in various applications including coupling digital microfluidics to electrospray mass spectrometry[33] and for the generation of liposomes.[34] The internal geometry of the 3D printed eductor can be seen in Figure S-4 A in the Supporting Information and consists of two coaxial nozzles nested such that compressed air flowed through the internal nozzle entrains flow through the external nozzle, generating modest vacuum pressure to induce flow within the capillary. As highlighted by the benefits of two-point detection for TDA, stable continuous flow rates are essential for accurate TDA. Figure 1A illustrates static vacuum pressure vs time for a mechanical diaphragm pump (blue) as compared to that achieved by the 3D printed eductor (black). A 30-fold improvement in the stability of static pressure was observed for the 3D printed eductor (0.05% RSD) as compared to the mechanical pump (1.53% RSD). Figure 1B shows that

https://doi.org/10.1021/acs.analchem.1c04566
Anal. Chem. 2022, 94, 6089−6096

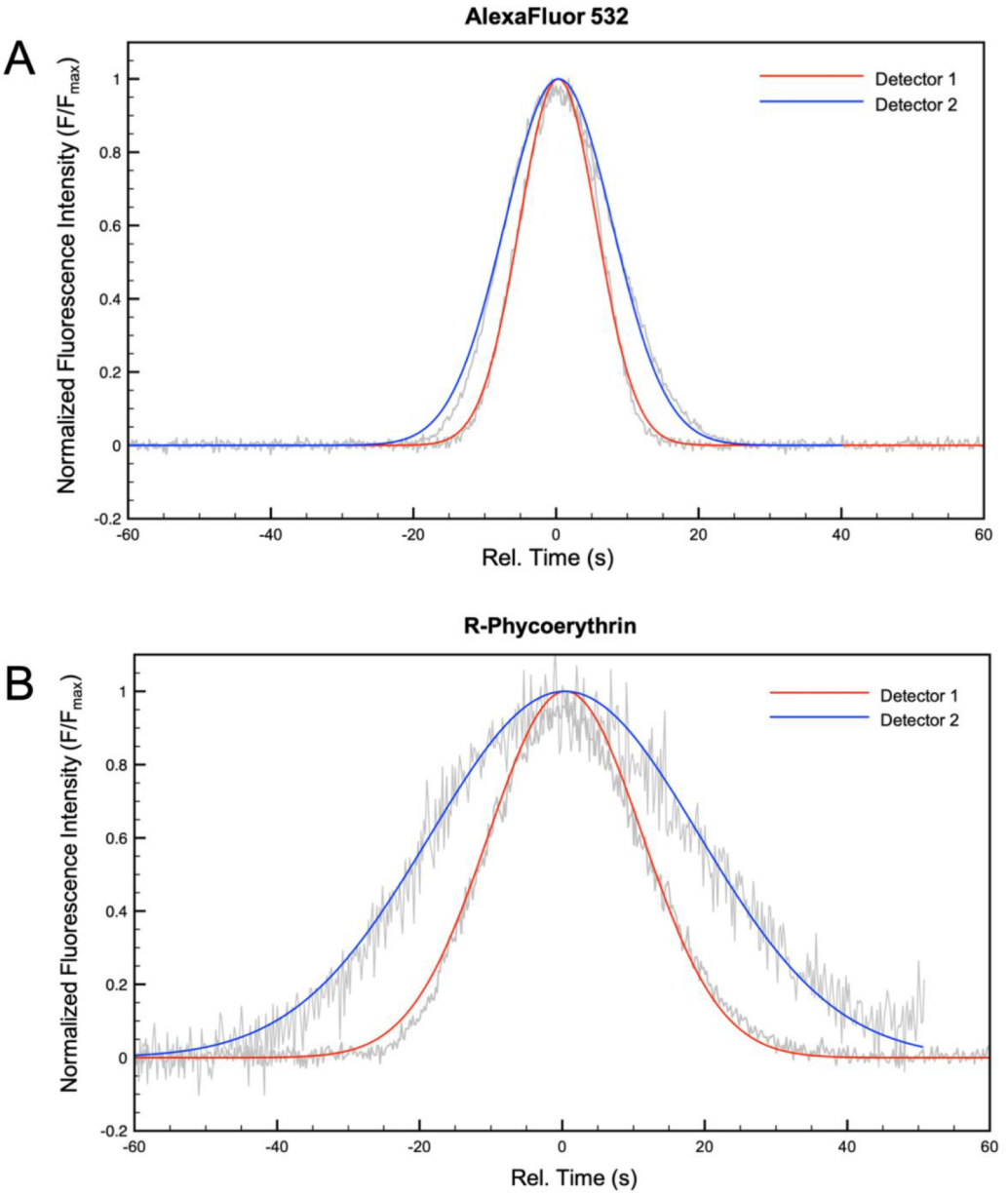

Figure 4. Dual-point detection TDA of (A) AlexaFluor 532 (20 nM) and (B) R-PE (5 nM). Raw data (gray) Gaussian fits (red and blue) are each normalized to a relative fluorescence scale, and the peaks are aligned on the time axis to illustrate relative differences in band broadening between the two model fluorophores. Peak arrival times were 72.2 and 168.3 s at detectors 1 and 2, respectively, for AlexaFluor 532, and 73.6 and 170.2 s at detectors 1 and 2, respectively, for R-Phycoerythrin.

highly stable static pressures (RSD < 0.1%) were produced with the eductor system across a range of static vacuum pressures from 0.2 to 1.7 psi below ambient pressure. Ultimately, the eductor system must provide precise control of vacuum pressures to allow flow conditions to be tuned to meet Taylor conditions for various analyses. Figure S-4B in the Supporting Information shows the resultant static vacuum pressure as a function of the volumetric flow rate of compressed air applied to the eductor inlet (R^2 = 0.997). Precise control of static pressure produced by the eductor enabled precise control of flow rates in the capillary for TDA experiments.

Optimized Design of the LIF Detection System. To reduce the collection of scattered excitation light, the optical design collects fluorescence emission 90° from the excitation path, as illustrated in Figure 2. Two LIF detectors of identical configuration were integrated into the instrument design. Each detector consisted of a housing to mount a low-cost 532 nm diode laser module as an excitation source and a concave mirror and ball lens as the primary optics for collecting fluorescence emission. The mirror and ball lens were positioned to collimate collected emission light, which was transmitted via a conventional 25 mm lens tube to a PMT for signal transduction. The PMT was fitted with a planoconvex lens to focus collimated emission light onto the PMT active area and a 532 nm notch filter to selectively reduce the intensity of scattered excitation light. Despite the notch filter fitted at the PMT, aberrant scatter of the laser sources was a significant hurdle to achieving appropriate fluorescent detection limits with this detector design. Therefore, we set out to optimize the detector design to reduce scatter and improve overall S/N for detected fluorescence signals.

https://doi.org/10.1021/acs.analchem.1c04566
Anal. Chem. 2022, 94, 6089−6096

Using a 500 nM Rhodamine 6G solution as a model fluorophore, we observed the resultant S/N for various emission axis design configurations termed designs A−D (see Supporting Information, Figure S-5). In addition to the PMT outfitted with a focusing lens (PCX, FL = 50 mm) and notch filter (533/17 nm, OD 6), the emission axis initially included the appropriate bandpass filter (580 ± 2, fwhm 10 ± 2 nm OD 6); however, in this configuration the net signal of fluorescence and background exceeded the dynamic range of the PMT. Thus, the first design modification that we evaluated, termed "Design A", added a neutral density filter (OD 0.9) to attenuate overall signal intensity to within the dynamic range of the PMT. This OD value was selected based on observing S/N with 500 nM Rhodamine 6G for various OD values (Supporting Information, Figure S-6). In an attempt to further selectively reduce the effect of laser scatter, Design B added a long-pass filter (550 nm, OD 6). Design C added an additional notch filter (532 nm, OD 5), resulting in a dramatic decrease in background intensity and a commensurate increase in S/N. Since the majority improvement in S/N from design A to Design C appeared to be attributed to the additional notch filter, Design D evaluated simplifying the emission axis by removing the long-pass filter. Surprisingly, this resulted in a dramatic reduction of S/N and led us to conclude that the maximum filtering approach (i.e., Design C) was optimal among the conditions we evaluated. The results of emission axis optimization are shown in Figure 3A. Although these results imply that further filtering may have resulted in continued improvements of S/N, in our judgment, the added cost of additional filtering was counter to the intended purpose of producing an accessible TDA instrument, and we anticipated that the sensitivity provided by Design C would be sufficient to achieve practical detection limits for various common fluorophores in this wavelength regime. Still, more work in this area may further improve S/N in this LIF detector design.

The design of the excitation optical axis was also considered on the basis of maximizing signal intensity and reducing laser scatter. A 9 mm diameter plano-convex lens (FL = 20 mm) was positioned in the excitation path to focus the laser onto the capillary detection window, maximizing incident intensity for fluorescence excitation. We evaluated spatial filtering of the laser source with pinholes of various diameters (0.4−2.5 mm) as a means to reduce the intensity of scattered excitation light collected in the emission axis. The pinholes were positioned between the laser source and the focusing lens to effectively attenuate the beam diameter of the laser, and S/N and background intensity were investigated as a function of the pinhole diameter (Figure 3B). Unsurprisingly, we observed increased background due to scatter with increasing beam diameter. Similarly, we observed increasing fluorescent signal with increasing beam diameter (data not shown), as the increased beam diameter represented an increase in excitation intensity at the focused detection point. Increases in both signal and noise were balanced at an optimal S/N with a pinhole diameter of 1.5 mm. This spatial filter was then incorporated into the final 3D printed geometry of the instrument.

LIF Detection Limits. To evaluate the efficacy of the LIF detection system for various applications, we produced calibration curves for four common fluorescent molecules compatible with 532 nm excitation: Rhodamine 6G, R-PE, AlexaFluor 532, and CF532 (Supporting Information, Figure S-7). In each case, we observed a linear response over at least one decade of dynamic range. Importantly, these experiments were designed to characterize detection limits, and thus, further work would be needed to evaluate the full linear and dynamic ranges for each fluorophore. The calculated LODs, based on linear regression of the calibration data, were 15 nM, 80 pM, 1 nM, and 5 nM, for Rhodamine 6G, R-PE, AlexaFluor 532, and CF532, respectively. These detection limits offer the prospect of analyte sizing by TDA at low and sub-nM analyte concentrations.

Validation of TDA Using Model Fluorescent Molecules. The printed capillary cartridge and alignment tool were used to prepare a 100 μm i.d. capillary with 15 cm detection window spacings for a TDA demonstration on AlexaFluor 532 and R-PE. Operating at a flow rate within the TDA regime, sample plugs were injected into the capillary, and the corresponding peaks were fitted to a Gaussian function. Figures 4A and B illustrate the differences in band broadening between AlexaFluor and R-PE, respectively. Raw data traces (gray) and Gaussian fits for detector 1 (red) and detector 2 (blue) were normalized, and the peak maxima aligned on the x-axis to better illustrate the relative degree of band broadening. TDA of AlexaFluor 532 determined an R_H of 0.87 ± 0.35 nm (n = 5). Notably, a small degree of peak asymmetry can be observed in raw data traces of Figures 4A and B, the source of which was not obvious. Peak asymmetry was neglected when it was sufficiently low so as not to interfere with Gaussian fitting. In other sample systems, such as synthetic lipid vesicles, more dramatic peak asymmetry was observed (see Supporting Information, Figure S-8), in which case Gaussian fits were somewhat poor, and TDA results were not considered reliable.

TDA was performed with 10 nM, 5 nM, 1 nM, and 750 pM R-PE providing R_H values of 5.48 ± 0.40 nm (n = 11), 5.64 ± 0.3 nm (n = 13), 5.75 ± 0.14 nm (n = 12), and 4.87 ± 0.98 nm (n = 14), respectively (Supporting Information, Figure S-9). We attribute the large variance in measured R_H at 750 pM to imprecision of the Gaussian fit resulting from a relatively low S/N. As a result, the 750 pM data was statistically different from the 1 nM data at the 95% confidence level. Still, the median result of the 750 pM data set was 5.03 nm, which represents a 10.7% error from the population mean observed across all other concentrations (5.63 nm), and suggests somewhat effective protein sizing even at sub-nM concentrations. TDA agreed well with the findings of MacColl et al., who determined a hydrodynamic radius of 5.54 ± 0.18 nm for R-PE by DLS.[35]

CONCLUSION

Size characterization is important across many fields of materials science and especially for the analysis of biomacromolecules and pharmaceutical preparations. Shortcomings of common methodologies like DLS and SEC present a need for rapid, straightforward, sensitive, and inexpensive methods for size characterizations. TDA meets most of these needs, but it is commonly performed using expensive CE instrumentation with UV absorbance detection that substantially limits sensitivity. We have developed a low-cost 3D printed instrument for TDA in fused silica capillaries that enables two-point LIF detection with low nM to mid pM LODs. Further work remains to achieve LODs competitive with the highest sensitivity LIF systems. The system relies on low-cost 532 nm laser diode modules, which limit fluorophore selection to labels that are not optimum for the lowest possible fluorescent LODs. Additionally, the emission axis relies on multiple dielectric optical filters that significantly drive up the overall cost of the system. Future work in this area will focus on improved optical efficiency and achieving more effective scatter rejection at reduced cost via spatial and spectral filtering.

https://doi.org/10.1021/acs.analchem.1c04566
Anal. Chem. 2022, 94, 6089−6096

The integration of an eductor-based pressure system enabled precision flow rate control with exceptional pressure stability, which is needed for accurate TDA. Since the pressure system is completely 3D printed and includes no moving parts, it presents a robust and exceptionally low-cost approach to pressure-driven flow for capillary-based analyses. Ultimately, the instrument was shown to be effective for protein sizing at low-to-sub nM concentrations. We anticipate that making this instrument available via digital distribution of the 3D printable models will facilitate wider access to the powerful sizing capabilities of TDA.

■ ASSOCIATED CONTENT

Supporting Information

The Supporting Information is available free of charge at https://pubs.acs.org/doi/10.1021/acs.analchem.1c04566.

Additional experimental details, photographs of component assemblies, and additional data plots (PDF)

■ AUTHOR INFORMATION

Corresponding Author

Christopher A. Baker − *Department of Chemistry and Biochemistry, New Mexico State University, Las Cruces, New Mexico 88003, United States;* orcid.org/0000-0001-9134-2994; Phone: 575-646-1015; Email: cabaker@nmsu.edu

Authors

Meagan R. Moser − *Department of Chemistry, University of Tennessee, Knoxville, Tennessee 37996, United States; Department of Chemistry and Biochemistry, New Mexico State University, Las Cruces, New Mexico 88003, United States*

Claire M. Smith − *Department of Chemistry and Biochemistry, New Mexico State University, Las Cruces, New Mexico 88003, United States*

Genoveve G. Gutierrez − *Department of Chemistry and Biochemistry, New Mexico State University, Las Cruces, New Mexico 88003, United States*

Complete contact information is available at: https://pubs.acs.org/10.1021/acs.analchem.1c04566

Notes

The authors declare no competing financial interest.

■ ACKNOWLEDGMENTS

This work was supported in part by the National Science Foundation under grant number CHE-2054748 and by the National Institute of General Medical Sciences of the National Institutes of Health under award number R35GM138173.

■ REFERENCES

(1) Moser, M. R.; Baker, C. A. *Analytical Methods* **2021**, *13*, 2357−2373.
(2) Stetefeld, J.; McKenna, S. A.; Patel, T. R. *Biophysical Reviews* **2016**, *8*, 409−427.
(3) Hawe, A.; Hulse, W. L.; Jiskoot, W.; Forbes, R. T. *Pharm. Res.* **2011**, *28* (9), 2302−2310.
(4) Arakawa, T.; Ejima, D.; Li, T.; Philo, J. S. *J. Pharm. Sci.* **2010**, *99* (4), 1674−1692.
(5) Ricker, R. D.; Sandoval, L. A. *J. Chromatogr. A* **1996**, *743* (1), 43−50.
(6) Ejima, D.; Yumioka, R.; Arakawa, T.; Tsumoto, K. *J. Chromatogr. A* **2005**, *1094* (1−2), 49−55.
(7) Neupane, R.; Källsten, M.; Lehmann, F.; Bergquist, J. *Analytical Methods* **2018**, *10*, 938−941.
(8) Neupane, R.; Bergquist, J. *Eur. J. Mass Spectrom.* **2017**, *23* (6), 417−426.
(9) Goyon, A.; Beck, A.; Veuthey, J.-L.; Guillarme, D.; Fekete, S. *J. Pharm. Biomed. Anal.* **2017**, *144*, 242−251.
(10) Taylor, G. *Proc. R. Soc. London, Ser. A* **1953**, *219*, 186−203.
(11) Giddings, J. C.; Seager, S. L. *J. Chem. Phys.* **1960**, *33*, 1579−1580.
(12) Hulse, W. L.; Forbes, R. T. *Int. J. Pharm.* **2011**, *411* (1−2), 64−68.
(13) Jensen, S. S.; Jensen, H.; Cornett, C.; Møller, E. H.; Østergaard, J. *J. Pharm. Biomed. Anal.* **2014**, *92*, 203−210.
(14) Leclercq, L.; Saetear, P.; Rolland-Sabaté, A.; Biron, J.-P.; Chamieh, J.; Cipelletti, L.; Bornhop, D. J.; Cottet, H. *Macromolecules* **2019**, *52*, 4421−4431.
(15) Ibrahim, A.; Meyrueix, R.; Pouliquen, G.; Chan, Y. P.; Cottet, H. *Anal. Bioanal. Chem.* **2013**, *405* (16), 5369−5379.
(16) Malburet, C.; Leclercq, L.; Cotte, J.-F.; Thiebaud, J.; Marco, S.; Nicolaï, M.-C.; Cottet, H. *Anal. Chem.* **2021**, *93* (16), 6508−6515.
(17) Chamieh, J.; Leclercq, L.; Martin, M.; Slaoui, S.; Jensen, H.; Østergaard, J.; Cottet, H. *Anal. Chem.* **2017**, *89* (24), 13487−13493.
(18) Sharma, U.; Gleason, N. J.; Carbeck, J. D. *Anal. Chem.* **2005**, *77*, 806−813.
(19) Chamieh, J.; Cottet, H. *J. Chromatogr. A* **2012**, *1241*, 123−127.
(20) Oukacine, F.; Morel, A.; Desvignes, I.; Cottet, H. *J. Chromatogr. A* **2015**, *1426*, 220−225.
(21) Chamieh, J.; Oukacine, F.; Cottet, H. *J. Chromatogr. A* **2012**, *1235*, 174−177.
(22) Casto, L. D.; Do, K. B.; Baker, C. A. *Anal. Chem.* **2019**, *91* (15), 9451−9457.
(23) Cheng, Y. F.; Dovichi, N. J. *Science* **1988**, *242* (4878), 562−564.
(24) Lada, M. W.; Vickroy, T. W.; Kennedy, R. T. *Anal. Chem.* **1997**, *69*, 4560−4565.
(25) Li, P.; Wang, L.; Guo, R.; Feng, H.; Ji, Y.; Lim, S. Y.; Ng, B. H.; Laserna, A. K. C.; Khan, S.; Chen, S.-M.; Li, S. F. Y. *Talanta* **2022**, *239*, 123061.
(26) Emonts, P.; Servais, A.; Ziemons, E.; Hubert, P.; Fillet, M.; Dispas, A. *ELECTROPHORESIS* **2021**, *42*, 1127−1134.
(27) Fu, J.-L.; Fang, Q.; Zhang, T.; Jin, X.-H.; Fang, Z.-L. *Anal. Chem.* **2006**, *78* (11), 3827−3834.
(28) Tao, L.; Kennedy, R. T. *Anal. Chem.* **1996**, *68* (22), 3899−3906.
(29) Schrell, A. M.; Mukhitov, N.; Yi, L.; Adablah, J. E.; Menezes, J.; Roper, M. G. *Anal. Methods* **2017**, *9* (1), 38−45.
(30) Zhang, N.; Zhang, H.-S.; Wang, H. *Electrophoresis* **2009**, *30* (13), 2258−2265.
(31) Jin, Z.; Chen, R.; Colón, L. A. *Anal. Chem.* **1997**, *69*, 1326−1331.
(32) Cottet, H.; Biron, J.-P.; Martin, M. *Analyst* **2014**, *139* (14), 3552−3562.
(33) Baker, C. A.; Roper, M. G. *Anal. Chem.* **2012**, *84* (6), 2955−2960.
(34) Sharifi, F.; Zhou, R.; Lim, C.; Jash, A.; Abbaspourrad, A.; Rizvi, S. S. H. *Journal of CO2 Utilization* **2019**, *29*, 163−171.
(35) MacColl, R.; Eisele, L. E.; Williams, E. C.; Bowser, S. S. *J. Biol. Chem.* **1996**, *271* (29), 17157−17160.